Available online at www.sciencedirect.com
ScienceDirect
Journal of Sound and Vibration 305 (2007) 672–688
JOURNAL OF SOUND AND VIBRATION
www.elsevier.com/locate/jsvi

Stability analysis of the Rijke tube with a Green's function approach

Maria A. Heckl[a,*], M.S. Howe[b]

[a]Department of Mathematics, Keele University, Staffordshire ST5 5BG, UK
[b]College of Engineering, Boston University, 110 Cummington Street, Boston, MA 02215, USA

Received 15 December 2006; received in revised form 6 April 2007; accepted 18 April 2007
Available online 8 June 2007

Abstract

An analysis is made of the stability of a Rijke tube. The tube is open at both ends and contains an acoustically compact flame holder that "blocks" the acoustic motions and across which there is a jump in the tube cross-sectional area. Oscillations are described in terms of an acoustic Green's function obtained in analytic form. The blocked motion near the flame holder can be regarded as incompressible; on either side of the flame holder full acoustic wave propagation is assumed. Velocity potentials of the incompressible and acoustic regions are matched by requiring continuity of pressure and volume flow. A linear heat release model is introduced that relates heat transfer from the flame to the acoustic field and provides the acoustic feedback necessary to maintain the oscillations. The oscillations can then be described in terms of the eigenmodes of an integral equation derived using the Green's function. Growth rates predicted from this equation are expressed in terms of properties of the heat release model.

1. Introduction

An unsteady source of heat within a cavity can be a source of intense acoustic waves. The Rijke tube is probably one of the simplest such examples. It consists of a vertical and straight open-ended tube with a heat source, typically a hot gauze or a flame, inside it. The sound is generated by a feedback mechanism involving a periodic transfer of heat between the heat source and air drawn up through the tube by convection, leading to an oscillation whose amplitude is determined by nonlinear mechanisms.

There is an extensive literature on the Rijke tube and related devices; see, for example the review by Raun et al. [1]. The Rijke tube derives its name from the 19th-century Dutch scientist Rijke [2], who discovered that a vertical tube with a hot gauze in the lower half would make a loud noise, whereas the tube was silent if the gauze was in the upper half. Various explanations and models for this phenomenon have been proposed since then, most notably by Rayleigh [3], who derived a general criterion for the excitation of heat-driven oscillations. Recent studies by Lighthill and Ffowcs Williams [4] and by Heckl [5] have involved stability analyses for specific cases, such as for a tube with a hot-wire gauze whose heat release characteristic is known from boundary layer theory.

*Corresponding author. Tel.: +44 1782 583423; fax: +44 1782 584268.
E-mail addresses: m.a.heckl@keele.ac.uk (M.A. Heckl), mshowe@bu.edu (M.S. Howe).

0022-460X/$ - see front matter © 2007 Elsevier Ltd. All rights reserved.
doi:10.1016/j.jsv.2007.04.027

In this paper, a new stability analysis of the Rijke tube is discussed, based on an acoustic analogy equation with a heat source term. This is combined with the Rijke tube's Green's function to obtain an integral equation. This approach has the advantage that it is readily extended to include additional sources that can influence the acoustics of the tube, such as the presence of vorticity and mean density variations (temperature "hot spots") within the flow, and the action of an active control system.

The Green's function and the eigenfrequencies of the tube with non-uniform mean temperature are calculated in Section 2. The integral equation is derived in Section 3 and analysed in Section 4 to extract equations for the modal amplitudes and growth rates of the oscillations with unsteady heating. Section 5 presents numerical solutions for the eigenfrequencies and for the stability behaviour of a particular Rijke tube. The relative advantages of the present approach are discussed in Section 6.

2. Green's function of the Rijke tube

2.1. Rijke tube configuration

We consider a Rijke tube with axisymmetric geometry; a cross-section between the tube axis and the tube wall is shown in Fig. 1. The tube has been turned sideways in this figure, i.e. the axial coordinate x denotes the vertical position, measured from the lower tube end at $x = 0$. The length of the tube is L, and a fuel line spans a length ℓ within the tube. There is a flame holder that introduces a blockage to the motion, where the tube cross-sectional area changes from $\mathscr{A}_1$ to $\mathscr{A}_2$. A small distance downstream of the flame holder, the mean temperature jumps from $\bar{T}_1$ to $\bar{T}_2$. The change in temperature causes the mean speed of sound to jump from c_1 to c_2. The tube ends are open with pressure nodes at $x = \ell_1$, just below the lower end ($\ell_1 < 0$), and at $x = \ell_2$, just above the upper end ($\ell_2 > L$).

The heat source has steady and unsteady components, each modelled as a point source (i.e. as a sheet spanning the cross-section of the tube and located at a point on the x-axis). The steady component is responsible for the jump in mean temperature. To keep the treatment general, the positions of the unsteady and steady heat source are taken to be independent. The effect of the unsteady source is discussed in Section 3; the current section considers the case of steady heating of the mean flow.

2.2. Analytical form of the Green's function

Green's function $G(\mathbf{x}, \mathbf{x}', t, t')$ is the velocity potential in the tube at position $\mathbf{x}$ and time t, created by an impulsive point source at position $\mathbf{x}'$ and time t'. It is the solution of

$$\frac{1}{c^2}\frac{\partial^2 G}{\partial t^2} - \nabla^2 G = \delta(\mathbf{x} - \mathbf{x}')\delta(t - t') \tag{1}$$

inside the tube, where $c = c(\mathbf{x})$ is the mean sound speed, and δ denotes the delta-function. $\mathbf{x}$ and $\mathbf{x}'$ are vectors in three-dimensional space; only their axial components, x and x', are of interest in most regions of the tube because the field there is one-dimensional, as will be shown in Section 2.3. G is required to vanish at $x = \ell_1$ and $x = \ell_2$; thus radiation losses from the ends are neglected. It has a normal derivative equal to zero on all internal surfaces and on the tube axis; it also satisfies the conditions of reciprocity and causality.

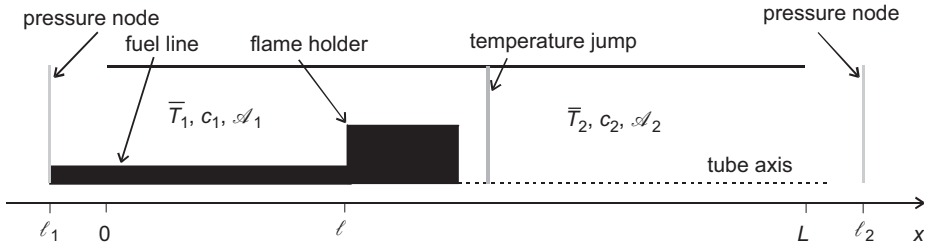

Fig. 1. Cross-section of the Rijke tube.

Green's function is calculated analytically in Sections 2.5 and 2.6, where it is shown to have the form

$$G(x,x',t-t') = \sum_{n=1}^{\infty} g_n(x,x')H(t-t')\sin\omega_n(t-t'). \tag{2}$$

H is the Heaviside function, ω_n are the eigenfrequencies of the Rijke tube (with steady heating) and g_n are the modal amplitudes. Green's function is an impulse response: it is zero before the impulse (at $t=t'$) and consists of a superposition of eigenmodes (numbered by the index n) thereafter.

2.3. The hydrodynamic and acoustic regions in the Rijke tube

The tube is divided into three regions as shown in Fig. 2: a hydrodynamic region (marked by grey shading) surrounds the flame holder, and there are two acoustic regions on either side of the hydrodynamic region.

In the hydrodynamic region the field is three-dimensional. This region is assumed to be small compared with the wavelength of low-order modes, so the acoustic motion can be treated as incompressible in this region. In the acoustic regions, the field is one-dimensional and acoustic waves are assumed to propagate.

For each mode of frequency ω ($\sim e^{-i\omega t}$), the velocity potential ϕ in the three regions can be written as

$$\phi = \begin{cases} a\sin\frac{\omega}{c_1}(x-\ell_1), & \text{acoustic region (cold)},\\ \alpha+\beta\varphi^*(\mathbf{x}), & \text{hydrodynamic region},\\ b\sin\frac{\omega}{c_2}(x-\ell_2), & \text{acoustic region (hot)}, \end{cases} \tag{3a,b,c}$$

where a,b,α and β are constants to be determined. The first and third expression in Eq. (3) represent harmonic waves, with a pressure node at $x=\ell_1$ and $x=\ell_2$, respectively. The second expression is an incompressible representation of the field in the hydrodynamic region, assuming the latter to be small compared with the acoustic wavelength.

φ^* is the velocity potential of the potential flow in the hydrodynamic region, normalized to have the following limiting values for its x derivative (the axial velocity)

$$\frac{\partial\varphi^*}{\partial x} \to \frac{\mathscr{A}_2}{\mathscr{A}_1} \quad \text{as} \quad x\to-\infty \quad \text{(to satisfy mass conservation)}, \tag{4a}$$

$$\frac{\partial\varphi^*}{\partial x} \to 1 \quad \text{as} \quad x\to\infty \quad \text{(normalization)}. \tag{4b}$$

The normal derivatives of φ^* are zero on the solid boundaries, the radial derivative vanishes at the tube axis, and φ^* satisfies the axisymmetric form of Laplace's equation. The motion is conveniently determined by considering the corresponding stream function ψ^*, which satisfies (see Ref. [6])

$$\frac{\partial^2\psi^*}{\partial x^2}+\frac{\partial^2\psi^*}{\partial r^2}-\frac{1}{r}\frac{\partial\psi^*}{\partial r}=0, \tag{5}$$

where r is the radial coordinate. Eq. (5) is readily solved by relaxation and finite differencing (see Ref. [7, pp. 652–653]), taking account of suitable conditions on the solid boundaries and of uniform inflow and

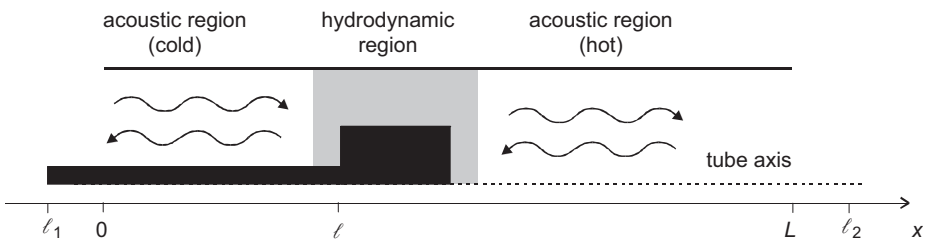

Fig. 2. Acoustic and hydrodynamic regions in the Rijke tube.

outflow conditions as $x \to \pm\infty$. This was done by Laws [8], and the field was visualized by plotting streamlines $\psi^* = \text{const}$. The case shown in Fig. 3 is for a geometry specified in Section 5.

The figure shows how the flow is distorted by the flame holder, and that the distortion is confined to a narrow region surrounding the flame holder. Thus the three-dimensional motion within the hydrodynamic region becomes one-dimensional at a small distance from the flame holder. We denote the axial position of the boundaries between one- and three-dimensional motion by X_1 (about 0.225 m for the case shown in Fig. 3) and X_2 (about 0.290 m for the same case) and regard these boundaries as interfaces between the acoustic regions and the hydrodynamic region. For simplicity we assume that the jump in mean temperature occurs at X_2; this limits the generality of our treatment, but still includes the typical case of a flame located a small distance downstream of the flame holder. The mean density is then uniform within each of the three regions; it is $\bar{\rho}_1$ in the upstream acoustic region and hydrodynamic region (i.e. for $0 < x < X_2$), and $\bar{\rho}_2$ in the downstream acoustic region (i.e. for $X_2 < x < L$).

The hydrodynamic region can be regarded as an airplug oscillating parallel to the x-axis. The conservation equations of volume flow and momentum across this airplug are

$$\mathscr{A}_1 u_1 - \mathscr{A}_2 u_2 = 0, \tag{6a}$$

$$p_1 - p_2 = \bar{\rho}_1 L_{\text{eff}} \frac{\partial u_2}{\partial t}. \tag{6b}$$

p_1 and u_1 are pressure and velocity respectively at the upstream interface (situated at X_1), and the equivalent quantities at the downstream interface (situated at X_2) are denoted by a subscript 2. L_{eff} is the effective length of the airplug [9, chapter 16], determined below in Section 2.4. The pressure and velocity are both continuous across the interfaces. The corresponding velocity potential at X_1 is ϕ_1. The velocity potential at X_2 jumps from ϕ_{2-} on the hydrodynamic side to ϕ_{2+} on the acoustic side, due to the jump in mean density from $\bar{\rho}_1$ to $\bar{\rho}_2$ at X_2.

2.4. The effective length of the airplug

An expression for the effective length can be derived by evaluating the momentum balance (6b) on the hydrodynamic side of the interfaces at X_1 and X_2, and combining it with the velocity potential φ^*. This is shown in detail in Appendix A.1. The result is

$$L_{\text{eff}} = \int_{X_2}^{\infty} \left(\frac{\partial \varphi^*}{\partial \xi} - 1 \right) \mathrm{d}\xi + \int_{-\infty}^{X_2} \left(\frac{\partial \varphi^*}{\partial \xi} - \frac{\mathscr{A}_2}{\mathscr{A}_1} \right) \mathrm{d}\xi + \frac{\mathscr{A}_2}{\mathscr{A}_1} (X_2 - X_1). \tag{7}$$

This expression must be evaluated numerically, using the results of the calculation plotted in Fig. 3,

$$\int_{X_2}^{\pm\infty} \frac{\partial \varphi^*}{\partial \xi} \mathrm{d}\xi = \int_{X_2}^{\pm\infty} \frac{1}{r} \frac{\partial \psi}{\partial r} \mathrm{d}\xi. \tag{8}$$

Both integrands in Eq. (7) are large near $\xi = X_2$, and approach zero exponentially fast with increasing distance from this point, hence the integration limits of $\pm\infty$ do not cause a problem numerically.

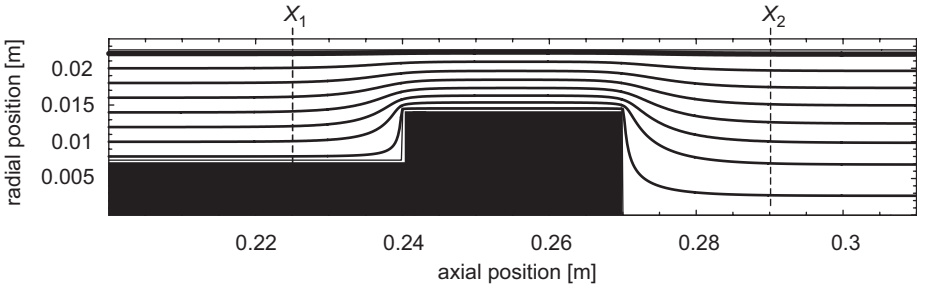

Fig. 3. Stream lines of potential flow in a tube section including the flame holder.

2.5. Eigenfrequencies

We return to the balance equations (6a) and (6b) and evaluate them on the acoustic side of the interfaces. The results can be written in terms of the velocity potentials ϕ_1 and ϕ_{2+} to give

$$\mathscr{A}_1 \frac{\partial \phi_1}{\partial x} - \mathscr{A}_2 \frac{\partial \phi_{2+}}{\partial x} = 0, \tag{9a}$$

$$\bar{\rho}_2 \phi_{2+} - \bar{\rho}_1 \phi_1 = \bar{\rho}_1 L_{\text{eff}} \frac{\partial \phi_{2+}}{\partial x}. \tag{9b}$$

ϕ_1 can be obtained from Eq. (3a), evaluated at $x = X_1$, and ϕ_{2+} from Eq. (3c), evaluated at $x = X_2$. Eqs. (9a) and (9b) then become

$$a \cos \frac{\omega}{c_1}(X_1 - \ell_1) - b \frac{\mathscr{A}_2}{\mathscr{A}_1} \frac{c_1}{c_2} \cos \frac{\omega}{c_2}(X_2 - \ell_2) = 0, \tag{10a}$$

$$a \sin \frac{\omega}{c_1}(X_1 - \ell_1) + b \left[L_{\text{eff}} \frac{\omega}{c_2} \cos \frac{\omega}{c_2}(X_2 - \ell_2) - \frac{\bar{\rho}_2}{\bar{\rho}_1} \sin \frac{\omega}{c_2}(X_2 - \ell_2) \right] = 0. \tag{10b}$$

The determinant of this 2×2 system of equations for a and b must vanish, and this yields

$$\begin{aligned} &- \frac{\bar{\rho}_2}{\bar{\rho}_1} \cos \frac{\omega}{c_1}(X_1 - \ell_1) \sin \frac{\omega}{c_2}(X_2 - \ell_2) \\ &+ \cos \frac{\omega}{c_2}(X_2 - \ell_2) \left[\frac{\mathscr{A}_2}{\mathscr{A}_1} \frac{c_1}{c_2} \sin \frac{\omega}{c_1}(X_1 - \ell_1) + L_{\text{eff}} \frac{\omega}{c_2} \cos \frac{\omega}{c_1}(X_1 - \ell_1) \right] = 0. \end{aligned} \tag{11}$$

This is a nonlinear equation for the frequency ω. It is best solved numerically, e.g. by the Newton–Raphson method with starting values $\omega_n^{(0)} = n\pi c_2/(\ell_2 - \ell_1)$, the eigenfrequencies of an open-ended uniformly hot tube without blockage or jump in cross-sectional area.

2.6. Modal amplitudes of Green's function

For the calculation of the Green's function and its amplitudes, we consider a point source at position x' in the hot acoustic region, as shown in Fig. 4. This particular case is relevant to the application discussed in Section 3.

At first the time-harmonic Green's function, $\hat{G}(x, x', \omega)$, is determined, which is the solution of

$$\frac{\partial^2 \hat{G}}{\partial x^2} + \frac{\omega^2}{c^2} \hat{G} = \delta(x - x'), \tag{12}$$

where $c = c_1$ for $0 < x < X_1$, and $c = c_2$ for $X_2 < x < L$. The time-dependent Green's function, $G(x, x', t - t')$, is then obtained by inverse Fourier transform. The calculations are quite lengthy, and full details are given in

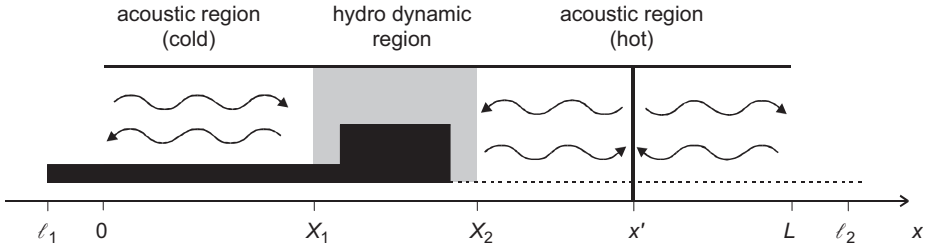

Fig. 4. Rijke tube with a point source.

Appendix A.2. The result for the modal amplitudes $g_n(x,x')$ in Eq. (2) is

$$g_n(x,x') = 2\frac{\hat{g}(x,x',\omega_n)}{\omega_n f'(\omega_n)}, \tag{13}$$

where

$$\hat{g}(x,x',\omega) = \begin{cases} A(x,\omega)C(x',\omega) & \text{for } 0<x<X_1, \\ D(x,\omega)C(x',\omega) & \text{for } X_2<x<x', \\ C(x,\omega)D(x',\omega) & \text{for } x'<x<L, \end{cases} \tag{14a,b,c}$$

with

$$A(x,\omega) = \sin\frac{\omega(x-\ell_1)}{c_1}, \tag{15a}$$

$$C(x,\omega) = \sin\frac{\omega(x-\ell_2)}{c_2}, \tag{15b}$$

$$D(x,\omega) = \frac{\bar{\rho}_1}{\bar{\rho}_2}\left(\sin\omega\tau_1 + \frac{\mathscr{A}_1 L_{\text{eff}}}{\mathscr{A}_2\ c_1}\omega\cos\omega\tau_1\right)\cos\frac{\omega(x-X_2)}{c_2} + \frac{\mathscr{A}_1 c_2}{\mathscr{A}_2 c_1}\cos\omega\tau_1\sin\frac{\omega(x-X_2)}{c_2}, \tag{15c}$$

and

$$\tau_1 = \frac{X_1-\ell_1}{c_1}, \quad \tau_2 = \frac{X_2-\ell_2}{c_2}. \tag{16a,b}$$

f' in Eq. (13) is the derivative of the function f that is defined in Eq. (A.18) and that specifies the eigenfrequencies, ω_n, by $f(\omega_n) = 0$.

3. Governing equations for the stability problem

3.1. Governing differential equation

We now consider a Rijke tube with an unsteady heat source. The velocity potential ϕ in the tube is governed by the acoustic analogy equation (see Ref. [10, p. 508])

$$\frac{1}{c^2}\frac{\partial^2\phi}{\partial t^2} - \frac{\partial^2\phi}{\partial x^2} = -\frac{\gamma-1}{c^2}q'(x,t). \tag{17}$$

q' is the fluctuating part of the heat release per unit mass of air (from the heat source to the air), and γ is the specific heat ratio; the speed of sound c takes values c_1 in the upstream region and c_2 in the downstream region.

In our configuration, the heat source is concentrated at the axial position x_q in the hot acoustic region. We assume a simple time-lag law, where the heat release q' depends linearly on the velocity fluctuation u' at an earlier time,

$$q'(x,t) = \frac{c^2}{\gamma-1}C_q u'(x,t-\tau)\delta(x-x_q). \tag{18}$$

This heat release characteristic is known to apply to hot gauzes (see Ref. [10, p. 511]) and to certain flames. τ is a time lag, and C_q is a measure of the strength of the heat source ($\tau>0$, $C_q\geqslant 0$). With $u' = (\partial\phi/\partial x)$ and Eqs. (17) and (18), we obtain the governing equation

$$\frac{1}{c^2}\frac{\partial^2\phi}{\partial t^2} - \frac{\partial^2\phi}{\partial x^2} = -C_q\frac{\partial\phi(x,t-\tau)}{\partial x}\delta(x-x_q). \tag{19}$$

This is a homogeneous equation and has the trivial solution $\phi(x,t) = 0$. Nontrivial solutions arise if the velocity potential is disturbed at some point in time, say at $t = 0$. Such a disturbance is typically described by imposing initial conditions, by specifying $\phi(x,t)|_{t=0}$ and $(\partial\phi/\partial t)|_{t=0}$.

Eq. (19) is now transformed into an integral equation involving the Green's function.

3.2. Integral equation for the acoustic velocity

Eq. (19) and the one-dimensional form of Eq. (1) are written in terms of the source variables x' and t'. Eq. (1) is multiplied by $\phi(x',t')$, Eq. (19) by $G(x,x',t-t')$, and the resulting equations are subtracted. This gives

$$\phi(x',t')\delta(x-x')\delta(t-t') + C_q G\frac{\partial\phi(x',t'-\tau)}{\partial x'}\delta(x'-x_q) = \frac{1}{c^2}\left(\phi\frac{\partial^2 G}{\partial t'^2} - G\frac{\partial^2\phi}{\partial t'^2}\right) - \left(\phi\frac{\partial^2 G}{\partial x'^2} - G\frac{\partial^2\phi}{\partial x'^2}\right). \tag{20}$$

This is integrated with respect to x' (from ℓ_1 to ℓ_2) and t' (from 0 to t). The result can be simplified (using the boundary conditions at the tube ends and causality, see Ref. [11]) to give the following integro-differential equation for ϕ:

$$\phi(x,t) = -C\int_{t'=\tau}^{t} G(x,x_q,t-t')\frac{\partial\phi(x',t'-\tau)}{\partial x'}\bigg|_{x'=x_q}\mathrm{d}t' - \frac{\varphi_0}{c^2}\frac{\partial G}{\partial t'}\bigg|_{\substack{x'=x_d\\t'=0}} + \frac{\dot\varphi_0}{c^2}G\bigg|_{\substack{x'=x_d,\\t'=0}} \tag{21}$$

where it has been assumed that

$$\phi(x,t)|_{t=0} = \varphi_0\delta(x-x_d), \tag{22a}$$

$$\frac{\partial\phi}{\partial t}\bigg|_{t=0} = \dot\varphi_0\delta(x-x_d). \tag{22b}$$

These initial conditions describe a disturbance at $t=0$, located at the axial position $x=x_d$. φ_0 and $\dot\varphi_0$ are a measure of the disturbance strength.

Eq. (21) can be turned into an integral equation for the velocity by differentiating with respect to x. Also, the lower integration limit can be changed to $t'=0$ by use of the Heaviside function. Evaluation at $x=x_q$ leads to an integral equation of the Volterra type [12] for the velocity at the heat source,

$$u_q(t) = -C_q\int_{t'=0}^{t}\frac{\partial G(x,x',t-t')}{\partial x}\bigg|_{\substack{x=x_q\\x'=x_q}} H(t'-\tau)u_q(t'-\tau)\mathrm{d}t' - \frac{\varphi_0}{c^2}\frac{\partial^2 G}{\partial x\partial t'}\bigg|_{\substack{x=x_q\\x'=x_d\\t'=0}} + \frac{\dot\varphi_0}{c^2}\frac{\partial G}{\partial x}\bigg|_{\substack{x=x_q\\x'=x_d\\t'=0}}, \tag{23}$$

where the abbreviation $u_q(t) = \partial\phi(x,t)/\partial x|_{x=x_q}$ has been introduced for the velocity at the heat source.

Eq. (23) can be solved numerically with an iteration scheme stepping forward in time, starting at $t=0$. However, more insight will be gained by an analytical approach; this is described in the next section.

4. Analytical solution of the governing integral equation

4.1. Amplitudes and complex eigenfrequencies

We assume that the velocity u_q is a superposition of modes for $t>\tau$ with amplitudes u_m and complex eigenfrequencies $\Psi_m = \Omega_m + \mathrm{i}\Delta_m$,

$$u_q(t) = \sum_{m=1}^{\infty}\left(u_m e^{-\mathrm{i}\Psi_m t} + u_m^* \mathrm{e}^{\mathrm{i}\Psi_m^* t}\right) \quad \text{for} \quad t>\tau. \tag{24}$$

Ω_m is the real eigenfrequency of mode m in the tube with unsteady heating (not to be confused with its equivalent ω_m for the tube with steady heating). The imaginary part of Ψ_m is the growth rate Δ_m; this indicates whether mode m is stable ($\Delta_m \leqslant 0$) or unstable ($\Delta_m > 0$). Once the modal properties u_m and Ψ_m are known, the stability behaviour can be predicted, and the detailed time history obtained from Eq. (24). The determination of u_m and Ψ_m requires several mathematical steps, which are outlined in Appendix A.3.

The following result is obtained for the complex eigenfrequencies Ψ_m,

$$1 = -C_q \sum_{n=1}^{\infty} \frac{\partial g_n(x_q, x_q)}{\partial x} \frac{\omega_n e^{i\Psi_m \tau}}{\omega_n^2 - \Psi_m^2}, \quad m = 1,\ 2,\ 3,\ \ldots. \tag{25}$$

These are nonlinear equations, one for each mode m.

For the amplitudes, two sets of linear equations for u_m and u_m* are obtained,

$$C_q \frac{\partial g_n(x_q, x_q)}{\partial x} \sum_{m=1}^{\infty} \left[\left(-\frac{\cos \omega_n \tau}{\omega_n^2 - \Psi_m^2} - \frac{i\Psi_m}{\omega_n} \frac{\sin \omega_n \tau}{\omega_n^2 - \Psi_m^2} \right) u_m + \left(-\frac{\cos \omega_n \tau}{\omega_n^2 - \Psi_m^{*2}} + \frac{i\Psi_m^*}{\omega_n} \frac{\sin \omega_n \tau}{\omega_n^2 - \Psi_m^{*2}} \right) u_m^* \right] = \frac{\varphi_0}{c^2} \frac{\partial g_n(x_q, x_d)}{\partial x}, \tag{26a}$$

and

$$C_q \frac{\partial g_n(x_q, x_q)}{\partial x} \sum_{m=1}^{\infty} \left[\left(i\Psi_m \frac{\cos \omega_n \tau}{\omega_n^2 - \Psi_m^2} - \omega_n \frac{\sin \omega_n \tau}{\omega_n^2 - \Psi_m^2} \right) u_m + \left(-i\Psi_m^* \frac{\cos \omega_n \tau}{\omega_n^2 - \Psi_m^{*2}} - \omega_n \frac{\sin \omega_n \tau}{\omega_n^2 - \Psi_m^{*2}} \right) u_m^* \right] = \frac{\dot{\varphi}_0}{c^2} \frac{\partial g_n(x_q, x_d)}{\partial x}, \tag{26b}$$

where $n = 1,2,3,\ldots$.

4.2. Approximate solution for the growth rate

An approximate analytical solution for the complex eigenfrequencies can be derived if the following assumptions are made:

$$\Omega_m \approx \omega_n \quad \text{for } n = m, \text{ but not for } n \neq m \tag{27a}$$

(steady and unsteady case have similar real eigenfrequencies),

$$|\Delta_m| \ll \Omega_m \quad \text{(small growth rates)}, \tag{27b}$$

$$\Omega_m \tau \ll 1 \quad \text{(time lag smaller than acoustic period of mode } m\text{)}. \tag{27c}$$

With Eqs. (27a) and (27b) the denominator of the term $(\omega_n e^{i\Psi_m \tau}/\omega_n^2 - \Psi_m^2)$ in Eq. (25) is small for $n = m$, but not for $n \neq m$, and thus the mth term dominates over all the others in the sum. This sum can then be approximated by the dominant term to give

$$1 + C_q \frac{\partial g_m(x_q, x_q)}{\partial x} \frac{\omega_m e^{i\Psi_m \tau}}{\omega_m^2 - \Psi_m^2} = 0. \tag{28}$$

For the low-order modes, Eq. (27c) is a reasonable assumption, and with that the approximation

$$e^{i\Psi_m \tau} \approx 1 + i\Psi_m \tau \tag{29}$$

can be made. Eq. (28) can then be turned into a quadratic equation for Ψ_m which has the following solutions:

$$\Psi_m = \frac{1}{2} \left(i\tau C_q \omega_m \frac{\partial g_m(x_q, x_q)}{\partial x} \pm \sqrt{-\left(\tau C_q \omega_m \frac{\partial g_m(x_q, x_q)}{\partial x} \right)^2 + 4\left(\omega_m^2 + C_q \omega_m \frac{\partial g_m(x_q, x_q)}{\partial x} \right)} \right). \tag{30}$$

If the term under the square root is negative, the real part of Ψ_m is zero. This describes the case where the velocity rises exponentially without oscillating. We ignore this case here and assume that the square-root term in Eq. (30) represents the real part of Ψ_m. Then

$$\Delta_m = \mathrm{Im}\, \Psi_m = \frac{1}{2} \tau C_q \omega_m \frac{\partial g_m(x_q, x_q)}{\partial x}, \tag{31a}$$

and

$$\Omega_m = \mathrm{Re}\Psi_m = \sqrt{\omega_m^2 + C_q\omega_m \frac{\partial g_m(x_q, x_q)}{\partial x} - \Delta_m^2}. \tag{31b}$$

Let us consider Δ_m, which indicates the stability behaviour of the heat-driven oscillation. Δ_m has four factors, three of which are positive:

$\tau > 0$ (otherwise the heat transfer would lead the velocity, rather than lag behind it)
$C_q > 0$ (in the case where the heat source is a wire gauze, $C_q < 0$ would describe the scenario of the surrounding air getting cooled, rather than heated, by the gauze; see the "Bosscha tube" described in Ref. [10, p. 512])
$\omega_m > 0$ for all $m = 1,2,3,\ldots$

Thus the sign of Δ_m is determined by the sign of the fourth factor, $\partial g_m(x_q, x_q)/\partial x$, and this depends on the position x_q of the heat source. We analyse the behaviour of $\partial g_m(x_q, x_q)/\partial x$ as a function of x_q numerically in the next section.

5. Numerical results

We consider a Rijke tube with the following geometry (see Fig. 5).

Tube length (L): 1 m
Inner tube radius (R): 0.0226 m
Length of flame holder (h): 0.03 m
Radius of flame holder: 0.0144 m
Radius of fuel line: 0.0076 m

These values correspond to our experimental Rijke tube arrangement.

The pressure nodes just outside the tube (determined by the Rayleigh end correction) are at a distance of $0.61R$ from the tube ends, giving

$$\ell_1 = -0.014\,\mathrm{m}, \quad \ell_2 = 1.014\,\mathrm{m}.$$

The ratio of downstream to upstream cross-sectional area is

$$\frac{\mathscr{A}_2}{\mathscr{A}_1} = 1.1128.$$

The effective length of the airplug has the value

$$L_{\mathrm{eff}} = 0.093\,\mathrm{m};$$

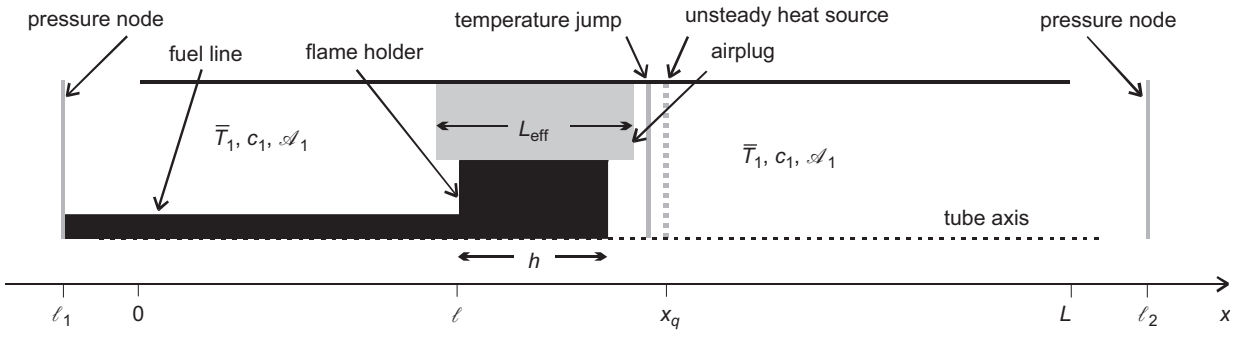

Fig. 5. Geometry of the Rijke tube.

this was calculated from Eq. (7), with $X_2 - X_1 = 0.065\,\mathrm{m}$. Although L_{eff} is surprisingly large, it is still much smaller than the wavelengths of the first few modes, which are of the order of 1 m. Hence the assumption in Section 2.3 (that the hydrodynamic region is acoustically compact) is still satisfied.

The mean temperature upstream of the heat source is room temperature. It jumps by 200 K across the heat source, i.e.

$$\bar{T}_1 = 288\,\mathrm{K}\ (\text{room temperature}), \quad \bar{T}_2 = 488\,\mathrm{K}.$$

The corresponding speeds of sound are

$$c_1 = 342\,\mathrm{m\,s^{-1}}, \quad c_2 = 446\,\mathrm{m\,s^{-1}}.$$

The source position x_q was increased in small steps from 0 to L. The hydrodynamic region was shifted accordingly, in such a way that x_q was a small constant distance of $0.01L$ downstream of this region, which had a constant length of 0.065 m. Thus its edges X_1 and X_2 (see Fig. 4) were at

$$X_2 = x_q - 0.01L, \quad X_1 = X_2 - 0.065\,\mathrm{m}.$$

The length of the fuel line was also increased in line with x_q, $\ell = X_1 + 0.015\,\mathrm{m}$.

The eigenfrequencies were calculated from Eq. (A.3). Their dependence on the heat source position x_q is shown in Fig. 6 for the first two modes. As x_q increases, the length of the cold region in the tube increases, while that in the hot region decreases. This would lead to a monotonic decrease of the eigenfrequencies (with increasing x_q) if the blockage and the jump in cross-sectional area were absent. Their presence disturbs the monotonic pattern and is responsible for the undulations in the curves of Fig. 6. ω_1 (black curve) fluctuates between 1295 and $1032\,\mathrm{s^{-1}}$ (206–164 Hz), and ω_2 (grey curve) between 2742 and $2074\,\mathrm{s^{-1}}$ (436–330 Hz).

Fig. 7 shows $\partial g_m(x_q, x_q)/\partial x$ as a function of x_q. The black curve is for the fundamental mode ($m = 1$), and the grey curve for the second mode ($m = 2$). The curves indicate that mode 1 is unstable in the range $0 < x_q < 0.469L$, and mode 2 in the ranges $0 < x_q < 0.246L$ and $0.413L < x_q < 0.722L$.

Our model assumes simple end conditions, neglecting losses due to acoustic radiation from the tube ends. As a consequence, the x_q ranges, for which instability is predicted, are slight over-estimates.

The predictions from our model are in line with the well-known observation that the fundamental mode of a Rijke tube is unstable if the heat source is in the lower half of the Rijke tube. The predicted stability behaviour for the second mode has also been observed.

The predictions are also in line with Rayleigh's criterion [3], which states that thermo-acoustic instabilities can occur if the phase difference between the rate of heat release q' and the sound pressure p is such that q' has its maximum during the high-pressure part of a cycle and its minimum during the low-pressure part of a cycle. Unstable oscillations are therefore only possible if $\overline{pq'} > 0$, where the time average (denoted by the over-bar)

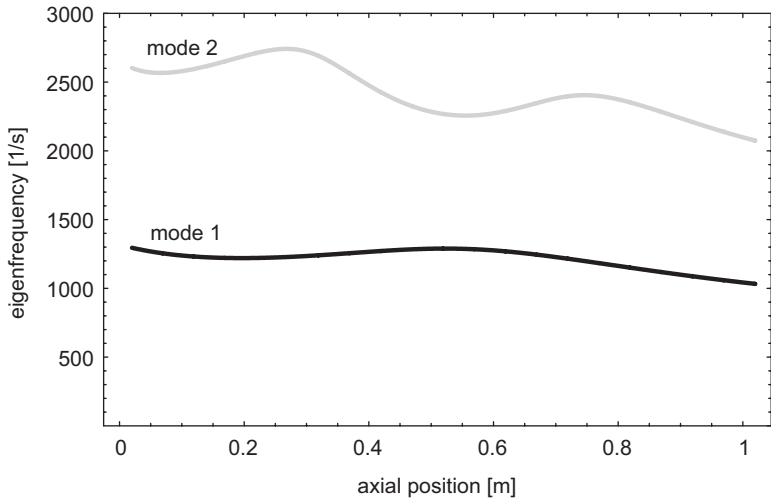

Fig. 6. Dependence of the eigenfrequencies ω_1 and ω_2 on the heat source position.

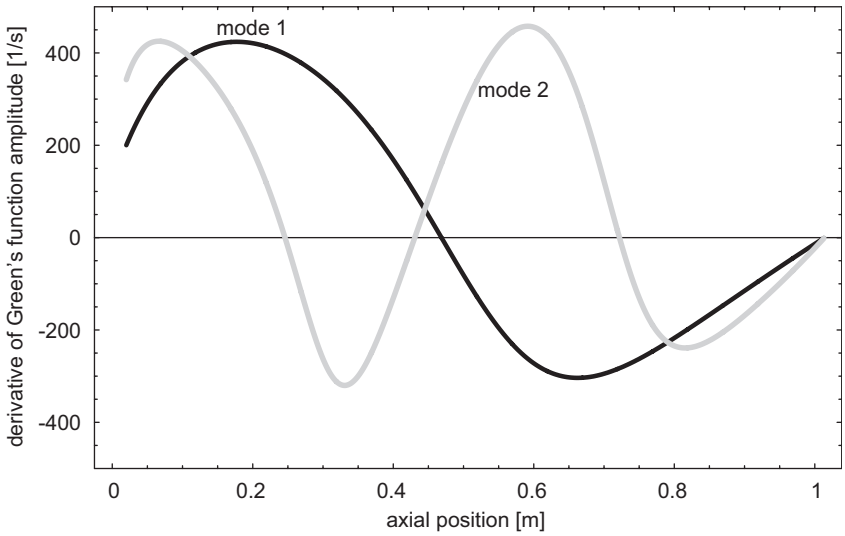

Fig. 7. Dependence of the derivatives of the Green's function amplitudes, $(\partial g_1(x_q, x_q)/\partial x)$ and $(\partial g_2(x_q, x_q)/\partial x)$ on the heat source position.

is evaluated over one period of the oscillation. For the fundamental mode of a simple tube (uniform cross-sectional area and uniform mean temperature, no blockage), this is the case if $0 < x_q < 0.5L$, the energy input to the sound being maximum when $x_q = 0.25L$ (see Ref. [10, Section 6.4.4]).

6. Conclusions and outlook

The Green's function approach presented in this paper predicts the stability behaviour of a Rijke tube with geometrical complications, in particular a blockage. Equivalent predictions can be made with simpler theories, for example with a classical control volume analysis, where balance equations for mass, momentum and energy across the heat source are formulated and analysed by an eigenvalue approach.

In contrast to other methods, our approach has several advantages: The acoustic analogy equation can readily be extended to include acoustic source processes, in addition to the heat release, such as vorticity or an active control system. An active control system, for example, that involves a sound source (within the tube or near one of its ends) can be simulated by adding a term to the right-hand side of Eq. (17), which represents a sound source coupled to the acoustic field in the tube. Heat release characteristics, other than the simple time-lag law used in this study, can be incorporated, for example the characteristic given by McIntosh and Rylands [13]. Furthermore, the heat release need not even be linear (as assumed in Section 3); an integral equation equivalent to Eq. (23) could be derived for a general nonlinear heat release characteristic and solved numerically by iteratively stepping forward in time, to give the time history of the acoustic velocity. This would show the transient behaviour, such as an amplitude increase during an instability, and also the long-term behaviour, such as convergence to a limit cycle. A further advantage is that our approach readily provides the effective length of the air surrounding the blockage; other approaches do not give this information.

As the Green's function is the response to excitation by an impulse, it is in principle possible to measure it. This would allow experimental validation of the Green's function we calculated theoretically. More generally, a measured Green's function could be incorporated into our approach to predict the stability behaviour of Rijke tubes whose geometry is too complicated for analytical treatment.

The Green's function of this paper is easily extended to include effects such as radiation losses at the tube ends. Similarly, the influence of the heat source being within or near the blocked region, where the flow is three-dimensional, could be incorporated using a Green's function for the special case where the unsteady heat source is in the hydrodynamic region of Fig. 4. Other tube geometries, more representative of practical devices, could also be treated. For example, an annular gas turbine combustor could, in a first approximation,

be represented by a "two-dimensional Rijke tube". Such a tube would have a wide, but thin rectangular cross-section and a heat source extending across the span of the tube. It would involve an analytic Green's function in two dimensions, obtained by extending the calculations in Section 2 from one to two dimensions.

Appendix A

A.1. The effective length of the airplug

We evaluate the momentum balance (6b) on the hydrodynamic side of the interfaces at X_1 and X_2, and write it in terms of the velocity potentials ϕ_1 and ϕ_{2-}, using

$$p_1 = -\bar{\rho}_1 \frac{\partial \phi_1}{\partial t}, \quad p_2 = -\bar{\rho}_1 \frac{\partial \phi_{2-}}{\partial t}, \quad u_2 = \frac{\partial \phi_{2-}}{\partial x}. \tag{A.1a,b,c}$$

This leads to

$$\phi_{2-} - \phi_1 = L_{\text{eff}} \frac{\partial \phi_{2-}}{\partial x}. \tag{A.2}$$

The velocity potentials are obtained by integrating Eqs. (4a, b) with respect to x and substituting the result into Eq. (3b) to give

$$\phi(x) = \alpha + \beta \frac{\mathscr{A}_2}{\mathscr{A}_1}(x - (X_1 - \bar{\ell}_1)) \quad \text{for } x \approx X_1, \tag{A.3a}$$

$$\phi(x) = \alpha + \beta(x - (X_2 - \bar{\ell}_2)) \quad \text{for } x \approx X_2. \tag{A.3b}$$

The integration constants have been chosen such that $\phi(X_1 - \bar{\ell}_1) = \phi(X_2 - \bar{\ell}_2) = \alpha$; $\bar{\ell}_1$ and $\bar{\ell}_2$ represent end corrections.

Evaluation of Eq. (A.3b) at $x = X_1$ and Eq. (A.3b) at $x = X_2$ gives ϕ_1 and ϕ_{2-}, and then Eq. (A.2) leads to

$$L_{\text{eff}} = \bar{\ell}_2 - \frac{\mathscr{A}_2}{\mathscr{A}_1}\bar{\ell}_1. \tag{A.4}$$

The effective length L_{eff} can be expressed in terms of the velocity potential φ^* by considering the limits $x \to \pm\infty$. As $x \to +\infty$,

$$\varphi^*(x) \to \begin{cases} \int_{X_2}^{\infty} \dfrac{\partial \varphi^*}{\partial \xi} \mathrm{d}\xi + \varphi^*(X_2) \quad \text{(identity)}, \\ x - (X_2 - \bar{\ell}_2) = \int_{X_2}^{x} \mathrm{d}\xi + \bar{\ell}_2 \quad \text{(from Eq. (A.3b))}. \end{cases} \tag{A.5a,b}$$

These two limits must be equal as $x \to +\infty$, hence

$$\bar{\ell}_2 = \int_{X_2}^{\infty} \left(\frac{\partial \varphi^*}{\partial \xi} - 1 \right) \mathrm{d}\xi + \varphi^*(X_2). \tag{A.6}$$

As $x \to -\infty$,

$$\varphi^*(x) \to \begin{cases} \int_{X_2}^{-\infty} \dfrac{\partial \varphi^*}{\partial \xi} \mathrm{d}\xi + \varphi^*(X_2) \quad \text{(identity)}, \\ \dfrac{\mathscr{A}_2}{\mathscr{A}_1}(x - (X_1 - \bar{\ell}_1)) = \dfrac{\mathscr{A}_2}{\mathscr{A}_1} \int_{X_2}^{x} \mathrm{d}\xi + \dfrac{\mathscr{A}_2}{\mathscr{A}_1}(-X_1 + X_2 + \bar{\ell}_1) \quad \text{(from Eq. (A.3a))}. \end{cases} \tag{A.7a,b}$$

Again, these two limits must be equal as $x \to -\infty$, giving

$$\frac{\mathscr{A}_2}{\mathscr{A}_1}(X_2 - X_1 + \bar{\ell}_1) = \int_{X_2}^{-\infty} \left(\frac{\partial \varphi^*}{\partial \xi} - \frac{\mathscr{A}_2}{\mathscr{A}_1} \right) \mathrm{d}\xi + \varphi^*(X_2). \tag{A.8}$$

Subtraction of Eq. (A.8) from Eq. (A.6), and use of Eq. (A.4) gives the expression for the effective length stated in Eq. (7) in the main text.

A.2. Modal amplitudes of Green's function

For the calculation of the Green's function and its amplitudes, we consider a point source at position x' in the hot acoustic region, as shown in Fig. 4.

At first we determine the time-harmonic Green's function, $\hat{G}(x,x',\omega)$, which is the solution of

$$\frac{\partial^2\hat{G}}{\partial x^2}+\frac{\omega^2}{c_1^2}\hat{G}=0 \quad \text{in } 0<x<X_1, \tag{A.9a}$$

and

$$\frac{\partial^2\hat{G}}{\partial x^2}+\frac{\omega^2}{c_2^2}\hat{G}=\delta(x-x') \quad \text{in } X_2<x<L. \tag{A.9b}$$

In the cold acoustic region, $\hat{G}$ is given by Eq. (3a). The hot acoustic region is subdivided by x' into two parts with forward and backward travelling waves in each. In summary,

$$\hat{G}(x,x',\omega)=\begin{cases} a\,\sin\,k_1(x-\ell_1) & \text{for } 0<x<X_1 \quad \text{(cold acoustic region)},\\ c\,\mathrm{e}^{\mathrm{i}k_2(x-X_2)}+d\,\mathrm{e}^{-\mathrm{i}k_2(x-X_2)} & \text{for } X_2<x<x' \quad \text{(hot acoustic region)},\\ b\sin k_2(x-\ell_2) & \text{for } x'<x<L \quad \text{(hot acoustic region)}. \end{cases} \tag{A.10a,b,c}$$

a,b,c and d are unknown coefficients, and $k_1=(\omega/c_1)$, $k_2=(\omega/c_2)$. The conditions across the hydrodynamic region apply as before (see Eqs. (9a) and (9b)), with ϕ_1 and ϕ_{2+} replaced by

$$\hat{G}_1=[a\sin k_1(x-\ell_1)]_{x=X_1}, \tag{A.11a}$$

and

$$\hat{G}_2=\left[c\,\mathrm{e}^{\mathrm{i}k_2(x-X_2)}+d\,\mathrm{e}^{-\mathrm{i}k_2(x-X_2)}\right]_{x=X_2}, \tag{A.11b}$$

respectively. This leads to the following two linear equations for a,c and d,

$$c+d=a\frac{\bar{\rho}_1}{\bar{\rho}_2}\left[\sin k_1(X_1-\ell_1)+L_{\mathrm{eff}}\frac{\mathscr{A}_1}{\mathscr{A}_2}k_1\cos k_1(X_1-\ell_1)\right], \tag{A.12a}$$

$$\mathrm{i}k_2c-\mathrm{i}k_2d=a\frac{\mathscr{A}_1}{\mathscr{A}_2}k_1\cos k_1(X_1-\ell_1). \tag{A.12b}$$

c and d can now be expressed in terms of a, to give

$$c=a\,\gamma, \tag{A.13a}$$

$$d=a\,\gamma^*, \tag{A.13b}$$

where

$$\gamma=\frac{1}{2}\left[\frac{\bar{\rho}_1}{\bar{\rho}_2}\sin k_1(X_1-\ell_1)+\frac{\bar{\rho}_1}{\bar{\rho}_2}\frac{\mathscr{A}_1}{\mathscr{A}_2}L_{\mathrm{eff}}k_1\cos k_1(X_1-\ell_1)-\mathrm{i}\frac{\mathscr{A}_1}{\mathscr{A}_2}\frac{k_1}{k_2}\cos k_1(X_1-\ell_1)\right], \tag{A.14}$$

and γ^* is the complex conjugate of γ. The expression for $\hat{G}(x,x',\omega)$ in Eq. (A.10b) can then be rewritten to give

$$\hat{G}(x,x',\omega)=2a[(\mathrm{Re}\,\gamma)\cos k_2(x-X_2)-(\mathrm{Im}\,\gamma)\sin k_2(x-X_2)], \tag{A.15}$$

for $X_2<x<x'$.

Using the Heaviside function H, it is possible to write $\hat{G}(x,x',\omega)$ for both parts of the hot acoustic region as

$$\begin{aligned}\hat{G}(x,x',\omega)=&\,2aH(x'-x)[(\mathrm{Re}\,\gamma)\cos k_2(x-X_2)-(\mathrm{Im}\,\gamma)\sin k_2(x-X_2)]\\&+bH(x-x')\sin\,k_2(x-\ell_2).\end{aligned} \tag{A.16}$$

a and b are determined to ensure that Eq. (A.16) satisfies Eq. (A.9b) in the hot acoustic region (see Ref. [14, pp. 43–44]). This involves differentiating Eq. (A.16) twice with respect to x, and using

$\mathrm{d}H(x-x')/\mathrm{d}x = \delta(x-x')$. Eq. (A.9b) then becomes an equation where the coefficients of $\delta(x-x')$ and its derivative $\delta'(x-x')$ on the left-hand side can be equated with those on the right. This leads to the following linear equations for a and b:

$$-2a[(\mathrm{Re}\,\gamma)\cos k_2(x'-X_2) - (\mathrm{Im}\,\gamma)\sin k_2(x'-X_2)] + b\sin k_2(x'-\ell_2) = 0, \tag{A.17a}$$

$$2ak_2[(\mathrm{Re}\,\gamma)\sin k_2(x'-X_2) + (\mathrm{Im}\,\gamma)\cos k_2(x'-X_2)] + bk_2\cos k_2(x'-\ell_2) = 1. \tag{A.17b}$$

The 2×2 determinant of these equations can be calculated and simplified to give

$$\det \equiv -\frac{\mathscr{A}_1}{\mathscr{A}_2}\frac{1}{c_1}\omega f(\omega),$$

where

$$f(\omega) = \frac{\mathscr{A}_1}{\mathscr{A}_2}\frac{1}{c_1}\left[-\cos\omega\tau_1\sin\omega\tau_2 + \frac{\bar{\rho}_1}{\bar{\rho}_2}\cos\omega\tau_2\left(\frac{\mathscr{A}_2}{\mathscr{A}_1}\frac{c_1}{c_2}\sin\omega\tau_1 + \frac{L_{\mathrm{eff}}}{c_2}\omega\cos\omega\tau_1\right)\right]. \tag{A.18}$$

a and b can then be found by Cramer's rule, and used to determine c and d from Eq. (A.13a,b).

If these results are combined with Eqs. (A.10a,b,c), $\hat{G}(x,x',\omega)$ assumes the compact form

$$\hat{G}(x,x',\omega) = \frac{\hat{g}(x,x',\omega)}{\omega f(\omega)}, \tag{A.19}$$

where

$$\hat{g}(x,x',\omega) = \begin{cases} A(x,\omega)C(x',\omega) & \text{for } 0<x<X_1, \\ D(x,\omega)C(x',\omega) & \text{for } X_2<x<x', \\ C(x,\omega)D(x',\omega) & \text{for } x'<x<L, \end{cases} \tag{A.20a,b,c}$$

with

$$A(x,\omega) = \sin\frac{\omega(x-\ell_1)}{c_1}, \tag{A.21a}$$

$$C(x,\omega) = \sin\frac{\omega(x-\ell_2)}{c_2}, \tag{A.21b}$$

$$D(x,\omega) = \frac{\bar{\rho}_1}{\bar{\rho}_2}\left(\sin\omega\tau_1 + \frac{\mathscr{A}_1}{\mathscr{A}_2}\frac{L_{\mathrm{eff}}}{c_1}\omega\cos\omega\tau_1\right)\cos\frac{\omega(x-X_2)}{c_2} + \frac{\mathscr{A}_1}{\mathscr{A}_2}\frac{c_2}{c_1}\cos\omega\tau_1\sin\frac{\omega(x-X_2)}{c_2}, \tag{A.21c}$$

and

$$\tau_1 = \frac{X_1-\ell_1}{c_1}, \quad \tau_2 = \frac{X_2-\ell_2}{c_2}. \tag{A22a,b}$$

The time-dependent Green's function is obtained from $\hat{G}(x,x',\omega)$ by the inverse Fourier transform,

$$G(x,x',t-t') = -\frac{1}{2\pi}\int_{-\infty}^{\infty}\hat{G}(x,x',\omega)\mathrm{e}^{-\mathrm{i}\omega(t-t')}\,\mathrm{d}\omega. \tag{A.23}$$

The integrand has singularities at the resonance frequencies, where $\omega=\omega_n$ (and also at $\omega=0$). This can be seen from the fact that the expression for $f(\omega)$ in Eq. (A.18) only differs by the constant factor $(\bar{\rho}_1/\bar{\rho}_2)(\mathscr{A}_1/\mathscr{A}_2)(1/c_1)$ from the left-hand side of Eq. (11), which is zero if $\omega=\omega_n$. The integral can therefore be evaluated by application of the residue theorem. Suitable integration paths are chosen for the cases $t<t'$ (before the source time t') and $t>t'$ (after the source time t') to ensure that causality is satisfied. For $t<t'$, the integration is along the real ω-axis, and a semicircular arc in the upper half-plane, without capturing the

singular points. For this case

$$G(x,x',t-t')=0,\ t<t'. \tag{A.24}$$

For $t>t'$, the integration is along the real ω-axis, and a semicircular arc in the lower half-plane, such that the singular points are enclosed. For this case

$$G(x,x',t-t')=\mathrm{i}\sum_{n=-\infty}^{\infty}\mathrm{Res}_{\omega_n}\left[\hat{G}(x,x',\omega)\mathrm{e}^{-\mathrm{i}\omega(t-t')}\right],\quad t>t'. \tag{A.25}$$

The residues at the simple poles ω_n ($n\neq 0$) can be calculated from the standard formula, given e.g. in Ref. [15, p. 158]. The residue at ω_0 turns out to be zero. Eq. (A.25) then becomes

$$G(x,x',t-t')=\mathrm{i}\sum_{\substack{n=-\infty\\ n\neq 0}}^{\infty}\frac{\hat{g}(x,x',\omega_n)}{\omega_n f'(\omega_n)}\mathrm{e}^{-\mathrm{i}\omega_n(t-t')},\quad t>t', \tag{A.26}$$

where f' is the derivative of the function f in Eq. (A.18). The frequencies ω_n have the symmetry property $\omega_{-n}=-\omega_n$. Taking into account the symmetry properties of the functions $\hat{g}(x,x',\omega)$ and $f'(\omega)$ with respect to ω, it is possible to reduce the sum over n to include only terms with positive n. The results (A.24) and (A.26) can be combined with the Heaviside function to give

$$G(x,x',t-t')=2H(t-t')\sum_{n=1}^{\infty}\frac{\hat{g}(x,x',\omega_n)}{\omega_n f'(\omega_n)}\sin\omega_n(t-t'). \tag{A.27}$$

Comparison of Eqs. (A.27) and (2) shows that the modal amplitudes of Green's function are given by

$$g_n(x,x')=2\frac{\hat{g}(x,x',\omega_n)}{\omega_n f'(\omega_n)}. \tag{A.28}$$

A.3. Modal amplitudes and complex eigenfrequencies

The aim is to extract equations for the modal properties u_m (amplitude) and Ψ_m (complex eigenfrequencies) of the heat-driven oscillation from Eq. (23). To this end, we Laplace transform (23) from the t-domain into the s-domain,

$$\begin{aligned}\mathscr{L}[u_q(t)]=&-C_q\mathscr{L}\left[\int_{t'=0}^{t}\left.\frac{\partial G(x,x',t-t')}{\partial x}\right|_{\substack{x=x_q\\ x'=x_q}}H(t'-\tau)u_q(t'-\tau)\mathrm{d}t'\right]\\ &-\frac{\varphi_0}{c^2}\mathscr{L}\left[\left.\frac{\partial^2 G}{\partial x\partial t'}\right|_{\substack{x=x_q\\ x'=x_d\\ t'=0}}\right]+\frac{\dot{\varphi}_0}{c^2}\mathscr{L}\left[\left.\frac{\partial G}{\partial x}\right|_{\substack{x=x_q\\ x'=x_d\\ t'=0}}\right],\end{aligned} \tag{A.29}$$

where the Laplace transform is defined in the standard way (see Ref. [16, p. 243]). The Laplace transform of the integral can be simplified by applying the convolution theorem and the shift theorem ([16, p. 243, entries 4 and 13]). The Laplace transforms of the Green's function derivatives are obtained by differentiating (2) and using

$$\mathscr{L}[\sin\omega_n t]=\frac{\omega_n}{s^2+\omega_n^2}, \tag{A.30a}$$

$$\mathscr{L}[\cos\omega_n t]=\frac{s}{s^2+\omega_n^2}, \tag{A.30b}$$

to transform the individual terms in the sum. Eq. (A.29) then becomes

$$\mathscr{L}[u_q(t)] = -C_q \sum_{n=1}^{\infty} \frac{\partial g_n(x_q, x_q)}{\partial x} \frac{\omega_n}{s^2+\omega_n^2} \mathrm{e}^{-s\tau} \mathscr{L}[u_q(t)] + \frac{\varphi_0}{c^2} \sum_{n=1}^{\infty} \frac{\partial g_n(x_q, x_d)}{\partial x} \frac{s\omega_n}{s^2+\omega_n^2} + \frac{\dot{\varphi}_0}{c^2} \sum_{n=1}^{\infty} \frac{\partial g_n(x_q, x_d)}{\partial x} \frac{\omega_n}{s^2+\omega_n^2}. \tag{A.31}$$

This is an algebraic equation for the Laplace transform of $u_q(t)$. Instead of solving it directly for $\mathscr{L}[u_q(t)]$, we substitute for $u_q(t)$ with Eq. (24), which has the Laplace transform

$$\mathscr{L}[u_q(t)] = \sum_{m=1}^{\infty} \left[\frac{u_m}{s+\mathrm{i}\Psi_m} + \frac{u_m^*}{s-\mathrm{i}\Psi_m^*} \right]. \tag{A.32}$$

Eq. (A.31) can then be written as

$$\sum_{m=1}^{\infty} \left[\frac{u_m}{s+\mathrm{i}\Psi_m} + \frac{u_m^*}{s-\mathrm{i}\Psi_m^*} \right] = -C_q \mathrm{e}^{-s\tau} \sum_{m=1}^{\infty} \sum_{n=1}^{\infty} \frac{\partial g_n(x_q, x_q)}{\partial x} \left[\frac{\omega_n u_m}{(s^2+\omega_n^2)(s+\mathrm{i}\Psi_m)} + \frac{\omega_n u_m^*}{(s^2+\omega_n^2)(s-\mathrm{i}\Psi_m^*)} \right] + \frac{1}{c^2} \sum_{n=1}^{\infty} \frac{\partial g_n(x_q, x_d)}{\partial x} \omega_n \frac{s\varphi_0 + \dot{\varphi}_0}{s^2+\omega_n^2}. \tag{A.33}$$

This can be transformed back from the s-domain into the t-domain, using Eq. (A.30a,b), the entries 4 on p. 243 and 5 on p. 245 in Ref. [16],

$$\mathscr{L}^{-1} \left[\frac{1}{(s^2+\omega_n^2)(s+\mathrm{i}\Psi_m)} \right] = \frac{1}{\omega_n^2 - \Psi_m^2} \left(-\cos\omega_n t + \frac{\mathrm{i}\Psi_m}{\omega_n} \sin\omega_n t + \mathrm{e}^{-\mathrm{i}\Psi_m t} \right), \tag{A.34}$$

and an equivalent formula for the complex conjugate to give

$$\sum_{m=1}^{\infty} \left(u_m \mathrm{e}^{-\mathrm{i}\Psi_m t} + u_m^* \mathrm{e}^{\mathrm{i}\Psi_m^* t} \right) = -C_q \sum_{m=1}^{\infty} \sum_{n=1}^{\infty} \frac{\partial g_n(x_q, x_q)}{\partial x} \frac{\omega_n u_m}{\omega_n^2 - \Psi_m^2} \left[\left(-\cos\omega_n(t-\tau) + \frac{\mathrm{i}\Psi_m}{\omega_n} \sin\omega_n(t-\tau) + \mathrm{e}^{-\mathrm{i}\Psi_m(t-\tau)} \right) + \frac{\omega_n u_m^*}{\omega_n^2 - \Psi_m^{*2}} \left(-\cos\omega_n(t-\tau) - \frac{\mathrm{i}\Psi_m^*}{\omega_n} \sin\omega_n(t-\tau) + \mathrm{e}^{\mathrm{i}\Psi_m^*(t-\tau)} \right) \right] + \frac{1}{c^2} \sum_{n=1}^{\infty} \frac{\partial g_n(x_q, x_d)}{\partial x} \omega_n \left[\varphi_0 \cos\omega_n t + \frac{\dot{\varphi}_0}{\omega_n} \sin\omega_n t \right]; \tag{A.35}$$

this is valid for all observer times $t > \tau$.

The basic functions of time in Eq. (A.35) are $\mathrm{e}^{-\mathrm{i}\Psi_m t}$, $\mathrm{e}^{\mathrm{i}\Psi_m^* t}$, $\cos\omega_n t$ and $\sin\omega_n t$. Further functions of time in this equation are

$$\mathrm{e}^{-\mathrm{i}\Psi_m(t-\tau)} = \mathrm{e}^{\mathrm{i}\Psi_m\tau}\, \mathrm{e}^{-\mathrm{i}\Psi_m t}, \tag{A.36a}$$

$$\mathrm{e}^{-\mathrm{i}\Psi_m^*(t-\tau)} = \mathrm{e}^{\mathrm{i}\Psi_m^*\tau}\, \mathrm{e}^{-\mathrm{i}\Psi_m^* t}, \tag{A.36b}$$

$$\cos\omega_n(t-\tau) = \cos\omega_n t \cos\omega_n\tau + \sin\omega_n t \sin\omega_n\tau, \tag{A.37a}$$

$$\sin\omega_n(t-\tau) = \sin\omega_n t \cos\omega_n\tau - \cos\omega_n t \sin\omega_n\tau, \tag{A.37b}$$

which can be expressed in terms of the basic functions as indicated. We use these in Eq. (A.35) to express this equation purely in terms of the basic functions and then equate their coefficients on the left and right-hand side of the equation. Equating the coefficients of $\mathrm{e}^{-\mathrm{i}\Psi_m t}$ gives Eq. (25), and equating those of $\mathrm{e}^{\mathrm{i}\Psi_m^* t}$ gives the complex conjugate of Eq. (25). Equating the coefficients of $\cos\omega_n t$ and $\sin\omega_n t$ gives Eqs. (26a) and (26b), respectively.

References

[1] R.L. Raun, M.W. Beckstead, J.C. Finlinson, K.P. Brooks, A review of Rijke tubes, Rijke burners and related devices, *Progress in Energy and Combustion Science* 19 (1993) 313–364.
[2] P.L. Rijke, Notiz über eine neue Art, die Luft in einer an beiden Enden offenen Röhre in Schwingungen zu versetzen, *Annalen der Physik* 107 (1859) 339–343.
[3] L. Rayleigh, The explanation of certain acoustical phenomena, *Nature* 18 (1878) 319–321.
[4] M.J. Lighthill, J.E. Ffowcs Williams, Demonstration of a shared lecture, *'Bulletin', Institute of Mathematics and its Applications* 7 (4) (1971) 3–10.
[5] M.A. Heckl, Active control from the noise of a Rijke tube, *Journal of Sound and Vibration* 124 (1988) 117–133.
[6] M. Heckl, Rijke tube without flame: Green's function and eigenfrequencies. Internal Report, Department of Mathematics, Keele University, 2004.
[7] W.H. Press, B.P. Flannery, S.A. Teukolsky, W.T. Vetterling, *Numerical Recipes*, Cambridge University Press, Cambridge, 1988.
[8] N.D. Laws, Calculation of irrotational flow past an axisymmetric flame holder in a cylindrical duct, Internal Report, College of Engineering, Boston University, 2004.
[9] L. Rayleigh, *The Theory of Sound, Volume Two*, Dover Publications, New York, 1877 re-issued 1945.
[10] M.S. Howe, *Acoustics of Fluid-Structure Interactions*, Cambridge University Press, Cambridge, 1998.
[11] M. Heckl, Rijke tube with unsteady heating from a hot gauze: stability analysis based on the Green's function, Internal Report, Department of Mathematics, Keele University, 2005.
[12] F.G. Tricomi, *Integral Equations*, Dover Publications, New York, 1957 re-issued 1985.
[13] A.C. McIntosh, S. Rylands, A model of heat transfer in Rijke tube burners, *Combustion Science and Technology* 114 (1996) 273–289.
[14] M.S. Howe, Mathematical methods for mechanical sciences, CD-Rom, Boston University, 2003.
[15] A.D. Osborne, *Complex Variables and Their Applications*, Addison Wesley Longman, Harlow, England, 1999.
[16] M.R. Spiegel, *Laplace Transforms, Schaum's Outline Series*, McGraw-Hill, New York, 1965.